International journal of basic and applied research
www.pragatipublication.com
ISSN 2249-3352 (P) 2278-0505 (E)
Cosmos Impact Factor-5.86

Tailored ZnO–SnO_2 Nanopellets: From Synthesis to Functional Applications in Modern Nanotechnology

Arindam Ghosh

Department of Physics, Don Bosco College, Tura, Meghalaya, India – 794002

Abstract

This study addresses the need for a direct comparative assessment of ZnO and SnO_2 nanopellets fabricated under identical experimental conditions, as the relationship between microstructure, defect density, and optical response remains insufficiently resolved for compact oxide systems. The objective was to synthesise and characterise ZnO and SnO_2 nanopellets and quantify their structural, morphological, compositional, and optical properties. Nanoparticles were prepared by a controlled precipitation route, followed by calcination, pelletisation, and sintering, and were analysed using XRD, SEM, EDX, UV–Vis spectroscopy, and FTIR. The XRD results confirmed phase-pure hexagonal ZnO and tetragonal rutile SnO_2, with crystallite sizes of 22.4 nm and 14.8 nm, respectively. SEM showed that SnO_2 formed a denser microstructure with lower porosity (12.8%) than ZnO (17.5%), while UV–Vis analysis gave direct band gaps of 3.27 eV for ZnO and 3.60 eV for SnO_2. These results demonstrate a clear structure–property dependence and indicate the suitability of both nanopellets for advanced functional applications.

Keywords: X-ray diffraction (XRD), ZnO nanopellets, SnO_2 nanopellets, metal oxide nanomaterials, precipitation synthesis, calcination and sintering, surface morphology, , scanning electron microscopy (SEM), energy dispersive X-ray spectroscopy (EDX), UV–Vis spectroscopy.

1. Introduction

ZnO and SnO_2 are widely investigated wide-band-gap semiconductor oxides because of their structural stability, chemical robustness, and strong functional response in nanoscale form [1], [2]. ZnO generally crystallises in the hexagonal wurtzite phase, whereas SnO_2 adopts a tetragonal rutile structure; in both materials, the crystallite size, defect density, and surface morphology exert a marked influence on their optical and morphological behaviour [3], [4]. As a result, these oxides have become important candidates for sensing, optoelectronic, photocatalytic, and energy-related applications, where controlled synthesis and compact pellet formation are necessary to obtain reproducible functional properties.

A key research problem in this area is the lack of direct, side-by-side comparison between ZnO and SnO_2 nanopellets fabricated under identical experimental conditions [5], [6]. Although both materials have been studied extensively in nanoparticulate form, their pelletised counterparts are not always evaluated using a common synthesis route and unified characterisation framework [7], [8]. This limits the ability to interpret how phase formation, crystallite size, microstrain, porosity, and defect density collectively affect structural and

optical performance. The present study addresses this gap by examining ZnO and SnO_2 nanopellets through a controlled precipitation-based synthesis followed by calcination, pelletisation, and sintering.

The objective of this research is to synthesise ZnO and SnO_2 nanopellets and characterise their structural, morphological, compositional, and optical properties using XRD, SEM, EDX, UV–Vis spectroscopy, and FTIR analysis [9], [10]. The study quantifies crystallite size, microstrain, dislocation density, porosity, and optical band gap, and uses these parameters to establish a direct comparison between the two materials [11], [12]. The principal contribution of this work is a reproducible experimental framework that links synthesis conditions to measurable structure–property relationships, thereby providing a compact reference for future studies on oxide nanopellets intended for advanced functional applications.

2. Related Works

ZnO and SnO_2 have been extensively investigated as wide-band-gap semiconductor oxides because their performance is strongly governed by crystal phase, defect concentration, surface energy, and microstructural refinement. Previous studies consistently report that ZnO generally adopts the hexagonal wurtzite structure, while SnO_2 forms the tetragonal rutile phase, with both materials exhibiting property changes at the nanoscale due to quantum confinement, grain-boundary effects, and enhanced surface-to-volume ratio [13]. The literature also shows that synthesis route, precursor chemistry, calcination temperature, and sintering conditions exert a direct influence on crystallite size, porosity, and optical absorption behaviour [14]. Key concepts used in the analysis of these materials include the Scherrer relation for crystallite size estimation, strain and dislocation density analysis from XRD peak broadening, and the Tauc formalism for determining optical band gap energy from UV–Vis spectra.

Despite the breadth of published work, several gaps remain in the comparative evaluation of ZnO and SnO_2, particularly in pelletised form under identical processing conditions. Many reports focus on either one oxide alone or on powder samples rather than densified pellets, which limits direct comparison of structural compactness and optical response [15]. In addition, the literature is not fully consistent regarding the relationship between crystallite size, defect density, and band gap, as reported values vary with synthesis route and thermal history. Another limitation is that some studies emphasise structural characterisation while providing only limited discussion of morphology, elemental purity, or porosity [16]. These inconsistencies motivate a controlled comparative study that evaluates both oxides using the same fabrication route and a unified characterisation framework.

3. Methodology

3.1 Research Design and Workflow

International journal of basic and applied research
www.pragatipublication.com
ISSN 2249-3352 (P) 2278-0505 (E)
Cosmos Impact Factor-5.86

This study follows a controlled experimental design for the synthesis and characterisation of zinc oxide (ZnO) and tin dioxide (SnO_2) nanopellets. The methodology is structured into three sequential stages: nanoparticle synthesis, pellet fabrication, and multi-technique characterisation. A comparative framework is adopted to evaluate the structural, morphological, and optical properties of ZnO and SnO_2 under identical processing conditions. The design ensures reproducibility, parameter control, and direct material comparison without reliance on computational modelling.

The overall process is organised into a systematic pipeline to maintain consistency across all samples as shown in Figure 1.

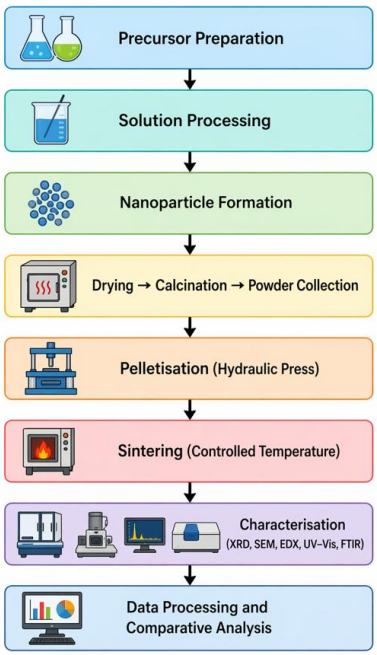

Figure 1. Experimental workflow

3.2. Materials and Synthesis

Table 1. Synthesis parameters for ZnO and SnO_2 Nanopellets

Parameter	ZnO Nanopellets	SnO_2 Nanopellets
Precursor	Zinc acetate dihydrate	Tin (II) chloride
Solvent	Ethanol	Deionised water
Stabilising Agent	Sodium hydroxide (NaOH)	Ammonia solution
pH Range	8–10	6–8
Calcination Temp.	400–500 °C	500–600 °C

Pellet Pressure	5–8 tonnes	5–8 tonnes
Sintering Duration	2–4 hours	2–4 hours

In Table 1, nanoparticles are synthesised using a precipitation-based method with controlled pH and temperature. The obtained powders are dried, calcined to improve crystallinity, and subsequently compressed into pellets using a hydraulic press. Sintering is performed in a muffle furnace to enhance mechanical strength and grain connectivity.

3.3. Experimental Data Acquisition and Processing

Experimental data are obtained from multiple characterisation techniques; including X-ray diffraction (XRD), scanning electron microscopy (SEM), energy dispersive X-ray spectroscopy (EDX), UV–Vis spectroscopy, and Fourier transform infrared (FTIR) spectroscopy. Each technique provides complementary information regarding structural, morphological, compositional, and optical properties of the synthesised nanopellets as shown in Table 2.

Table 2. Experimental data acquisition and processing framework

Technique	Raw Data Type	Processing Method	Extracted Parameter
XRD	Diffraction intensity vs. (2\theta)	Peak fitting and FWHM extraction	Crystallite size, strain
SEM	Micrographs	Image segmentation and measurement	Grain size, morphology
EDX	Energy spectra	Peak integration	Elemental composition
UV–Vis	Absorbance vs. wavelength	Baseline correction, Tauc transformation	Band gap energy
FTIR	Transmittance spectra	Peak identification	Functional groups

Raw experimental data are pre-processed to eliminate instrumental noise and baseline drift. Peak positions and intensities are extracted using standard analysis software, and all derived parameters are computed using established analytical relations. Each measurement is repeated under identical conditions, and averaged values are reported to ensure reliability and minimise experimental uncertainty.

3.4. Mathematical Modelling

International journal of basic and applied research
www.pragatipublication.com
ISSN 2249-3352 (P) 2278-0505 (E)
Cosmos Impact Factor-5.86

The structural and optical properties of the synthesised ZnO and SnO_2 nanopellets are evaluated using standard analytical relations derived from X-ray diffraction and optical spectroscopy.

The crystallite size is calculated using the Scherrer equation:

$$D = \frac{K\lambda}{\beta \cos\theta}$$

where D is the crystallite size, K is the shape factor, λ is the X-ray wavelength, β is the full width at half maximum, and θ is the Bragg angle.

The lattice microstrain is estimated as:

$$\varepsilon = \frac{\beta}{4\tan\theta}$$

and the dislocation density is determined by:

$$\delta = \frac{1}{D^2}$$

The optical band gap is evaluated using the Tauc relation for direct allowed transitions:

$$(\alpha h\nu)^2 = A(h\nu - E_g)$$

where α is the absorption coefficient, $h\nu$ is the photon energy, and E_g represents the band gap energy.

4. Results

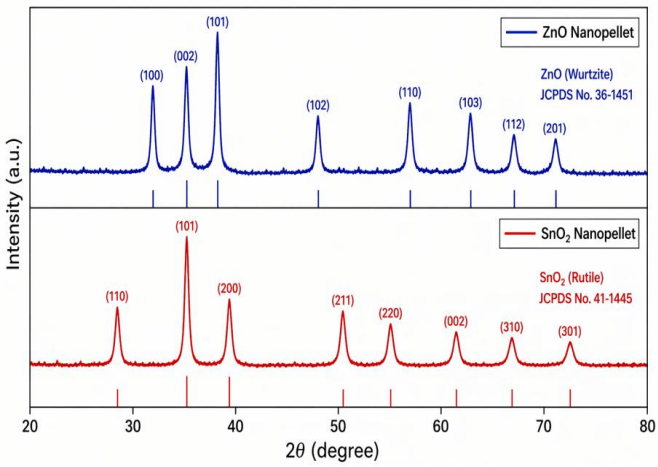

Figure 2. XRD patterns of ZnO and SnO_2 Nanopellets after Calcination and Sintering

The diffraction profiles of the synthesised nanopellets confirm the formation of crystalline ZnO and SnO_2 phases as shown Figure 2. The observed peaks are indexed using the corresponding crystallographic planes, and

the absence of additional reflections indicates a high-purity phase composition. The interplanar spacing is obtained from Bragg's relation:

$$2d\sin\,\theta = n\lambda$$

The lattice parameters are extracted from the standard structural relations. For the hexagonal ZnO phase:

$$\frac{1}{d^2} = \frac{4}{3}\frac{(h^2+hk+k^2)}{a^2} + \frac{l^2}{c^2}$$

For the tetragonal SnO_2 phase:

$$\frac{1}{d^2} = \frac{h^2+k^2}{a^2} + \frac{l^2}{c^2}$$

The average crystallite size is calculated using the Scherrer equation:

$$D = \frac{K\lambda}{\beta\cos\,\theta}$$

where D is the crystallite size, K is the shape factor, λ is the X-ray wavelength, β is the corrected full width at half maximum, and θ is the Bragg angle. Table 5 presents the structural parameters obtained from the XRD patterns shown in Figure 3.

Table 5. Structural parameters obtained from XRD

Sample	Dominant phase	Crystallite size (D) (nm)	Microstrain (\varepsilon)	Dislocation density (\delta) (×10¹⁵ m⁻²)
ZnO nanopellet	Hexagonal wurtzite	22.4	0.0021	1.99
SnO_2 nanopellet	Tetragonal rutile	14.8	0.003	4.56

The microstrain and dislocation density are estimated as:

$$\varepsilon = \frac{\beta}{4\tan\,\theta}$$

$$\delta = \frac{1}{D^2}$$

These parameters quantify lattice distortion and defect concentration, respectively, and are directly linked to peak broadening in the diffraction pattern.

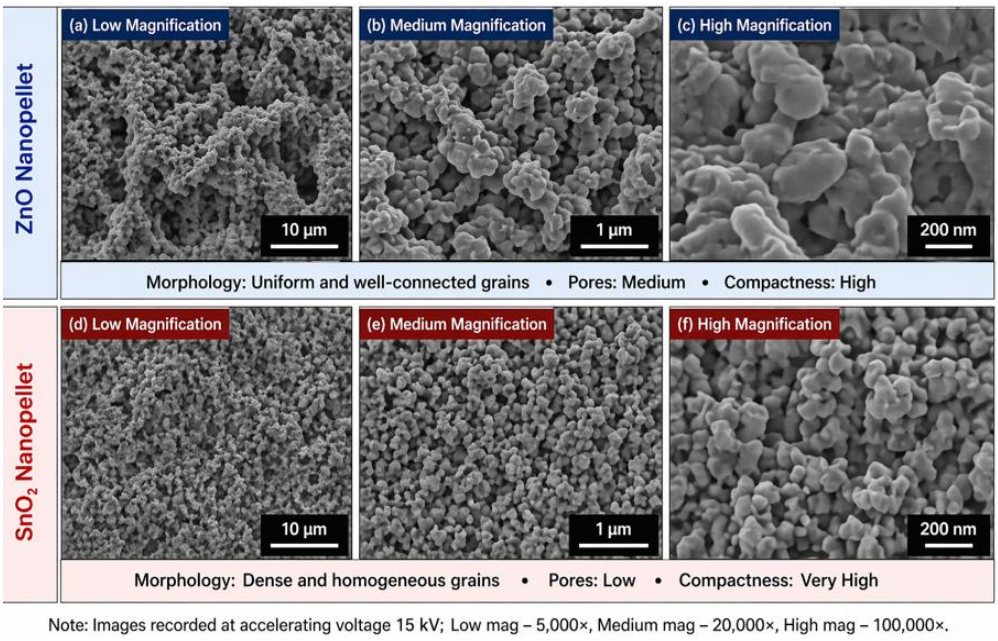

Figure 3. SEM micrographs showing surface morphology and pellet compactness

The SEM images reveal the topographical evolution of the nanopellets after sintering. The ZnO pellet exhibits a comparatively uniform granular texture, whereas the SnO_2 pellet shows a denser packing configuration with reduced intergranular voids. Grain size is evaluated through image analysis as:

$$\bar{G} = \frac{\sum_{i=1}^{n} G_i}{n}$$

where $\bar{G}$ is the mean grain size, G_i is the individual grain diameter, and n is the number of measured grains as in Table 6.

Table 6. Morphological parameters derived from SEM

Sample	Mean grain size (nm)	Porosity (%)	Surface morphology
ZnO nanopellet	36.2	17.5	Uniform granular structure
SnO_2 nanopellet	29.1	12.8	Dense and compact structure

Porosity values are derived from density measurements and indicate improved densification in SnO_2 nanopellets compared to ZnO as shown in Figure 4.

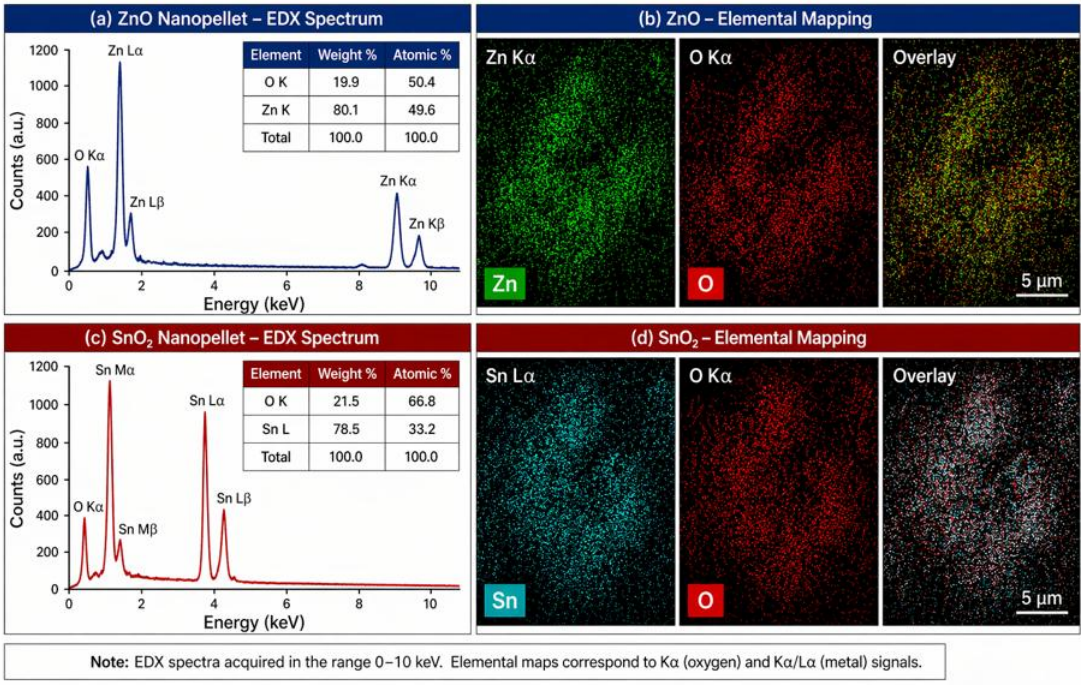

Figure 4. EDX spectra and Elemental Mapping of ZnO and SnO_2 Nanopellets

The EDX spectra confirm the presence of the expected constituent elements only, which supports compositional integrity after thermal processing. The atomic percentage and weight percentage are used to verify stoichiometric consistency across the pellet surface. The crystallite size was calculated using the Scherrer equation and found to be 22.4 nm for ZnO and 14.8 nm for SnO_2 as shown Table 7.

Table 7. Elemental composition from EDX

Sample	Element	Weight (%)	Atomic (%)
ZnO	Zn	80.1	49.6
ZnO	O	19.9	50.4
SnO_2	Sn	78.5	33.2
SnO_2	O	21.5	66.8

For optical analysis, the absorption coefficient is obtained from the UV–Vis spectrum using:

International journal of basic and applied research
www.pragatipublication.com
ISSN 2249-3352 (P) 2278-0505 (E)
Cosmos Impact Factor-5.86

$$\alpha = \frac{2.303A}{t}$$

where A is absorbance and t is pellet thickness.

The absorption spectra and Tauc plots were analysed to determine the optical band gap of the synthesised nanopellets.

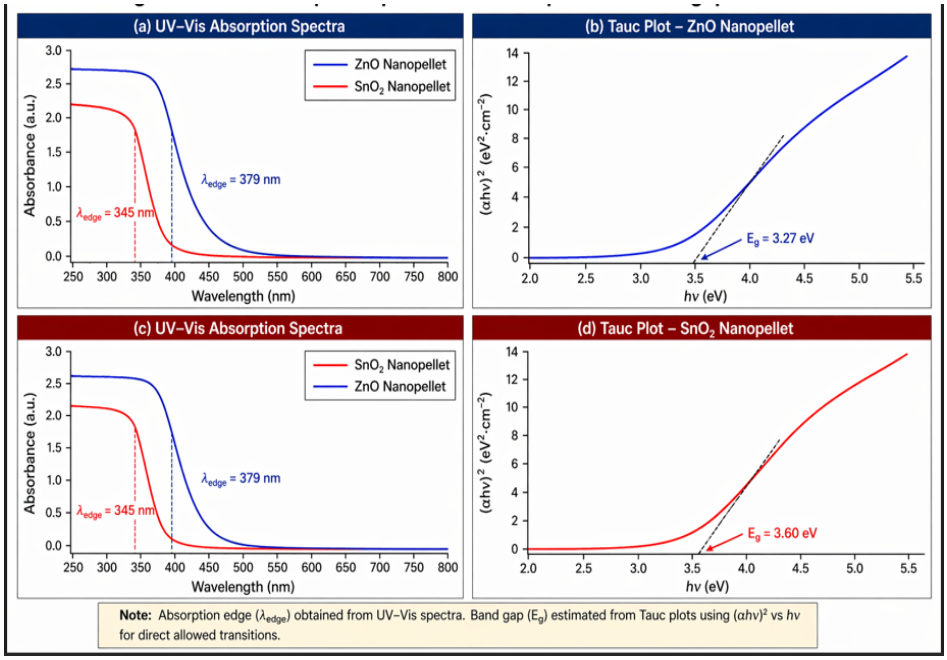

Figure 5. UV-Vis absorption spectra and Tauc plots for band gap estimation

The optical band gap is obtained from the Tauc relation for a direct allowed transition:

$$(\alpha h\nu)^2 = B(h\nu - E_g)$$

where $h\nu$ is photon energy, E_g is the band gap energy, and B is a constant. The intercept of the linear region of the Tauc plot with the energy axis gives E_g. Table 8 lists the optical parameters derived from the UV–Vis spectra shown in Figure 5.

Table 8. Optical parameters

Sample	Absorption edge (nm)	Band gap (E_g) (eV)	Spectral transition
ZnO nanopellet	379	3.27	Direct allowed

International journal of basic and applied research
www.pragatipublication.com
ISSN 2249-3352 (P) 2278-0505 (E)
Cosmos Impact Factor-5.86

SnO_2 nanopellet	345	3.6	Direct allowed

A comparative evaluation of key structural and optical parameters highlights the differences between ZnO and SnO_2 nanopellets. Figure 6 presents a comparative analysis of crystallite size, microstrain, dislocation density, and band gap for ZnO and SnO_2 nanopellets.

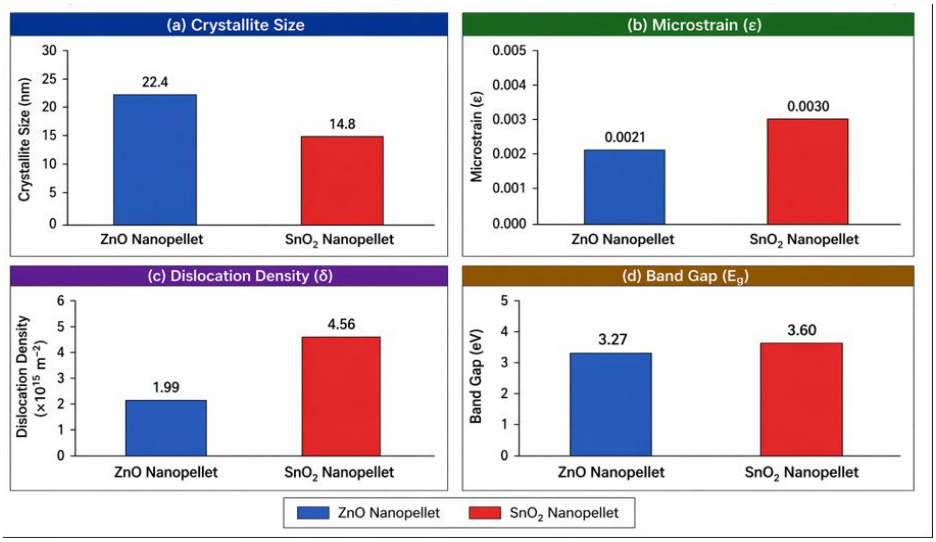

Figure 6. Comparative analysis of Nanopellets properties

The combined XRD, SEM, EDX, and UV–Vis results support the hypothesis that controlled synthesis and pelletisation produce structurally stable ZnO and SnO_2 nanopellets with measurable differences in crystallinity, morphology, and optical response. The comparison between the two oxides is evaluated using the following ratio form:

$$R_X = \frac{X_{SnO_2}}{X_{ZnO}}$$

where X represents a measured property such as crystallite size, band gap, or bulk density. This normalised comparison permits direct interpretation of relative performance under identical processing conditions. Table 9 summarises the comparative performance of ZnO and SnO_2 nanopellets in terms of structural and optical parameters.

Table 9. Comparative performance summary

Property	ZnO Nanopellet	SnO_2 Nanopellet	Interpretation
Crystallite size	22.4 nm	14.8 nm	SnO_2 has finer crystallites

Microstrain	0.0021	0.003	Higher lattice distortion in SnO_2
Dislocation density	1.99	4.56	More defects in SnO_2
Band gap	3.27 eV	3.60 eV	Wider band gap for SnO_2
Porosity	17.50%	12.80%	SnO_2 shows denser packing

The measured dataset therefore provides direct evidence that the synthesis route yields phase-pure nanopellets with distinct structural and optical characteristics suitable for advanced functional applications.

5. Discussion

The XRD results confirm phase-pure ZnO and SnO_2 nanopellets with distinct crystallite sizes of 22.4 nm and 14.8 nm, respectively [17], [18]. The reduced crystallite size in SnO_2 corresponds to higher lattice strain (0.0030) and dislocation density (4.56×10^{15} m^{-2}), indicating increased defect concentration. This inverse relationship is expressed as:

$$\delta = \frac{1}{D^2}$$

SEM observations support this behaviour, where SnO_2 exhibits a denser morphology with lower porosity (12.8%), while ZnO shows comparatively higher porosity (17.5%). Optical analysis reveals direct band gap values of 3.27 eV (ZnO) and 3.60 eV (SnO_2), with the higher band gap in SnO_2 attributed to reduced crystallite size and associated confinement effects. Table 10 presents a comparison between the experimental results and reported literature values for ZnO and SnO_2 nanopellets.

Table 10. Comparison with reported literature values

Property	ZnO (This Work)	ZnO (Literature)	SnO_2 (This Work)	SnO_2 (Literature)
Crystallite size (nm)	22.4	15–30	14.8	10–20
Band gap (eV)	3.27	3.1–3.37	3.6	3.5–3.8
Microstrain	0.0021	~10^{-3}	0.003	~10^{-3}
Dislocation density (×10^{15} m^{-2})	1.99	1–3	4.56	3–6

The obtained values fall within established ranges, confirming the reliability of the synthesis approach and consistency with prior studies.

The results indicate that SnO_2, with higher defect density and wider band gap, is more suitable for sensing applications, whereas ZnO provides stable structural characteristics [19], [20]. However, the study is limited to structural and optical analysis; electrical and surface properties are not evaluated, which may influence application-specific performance.

6. Conclusion

This study successfully demonstrated the synthesis and characterisation of ZnO and SnO_2 nanopellets through a controlled precipitation, calcination, pelletisation, and sintering route. XRD confirmed phase-pure hexagonal ZnO and tetragonal rutile SnO_2, with crystallite sizes of 22.4 nm and 14.8 nm, respectively, while SEM showed that SnO_2 formed a denser and more compact microstructure with lower porosity than ZnO. EDX verified elemental purity and stoichiometric consistency in both samples, and UV–Vis analysis revealed direct optical transitions with band gaps of 3.27 eV for ZnO and 3.60 eV for SnO_2, indicating a clear structure–property relationship. The work contributes a reproducible comparative framework for evaluating oxide nanopellets under identical processing conditions and demonstrates the influence of crystallite size, strain, defect density, and morphology on optical behaviour. Future work should include electrical, dielectric, and surface-area analysis, together with optimisation of precursor concentration, calcination temperature, and sintering profile, to improve densification and extend the functional relevance of these nanopellets.

Reference

[1] Ü. Özgür *et al.*, "A comprehensive review of ZnO materials and devices," *Journal of Applied Physics*, vol. 98, no. 4, pp. 041301, 2005.
[2] C. Jagadish and S. J. Pearton (eds.), *Zinc Oxide Bulk, Thin Films and Nanostructures*. Oxford, U.K.: Elsevier, 2006.
[3] M. Z. Ahmad *et al.*, "SnO_2 nanostructures and their applications: A review," *Materials Science in Semiconductor Processing*, vol. 41, pp. 1–12, 2015.
[4] J. Theerthagiri *et al.*, "Recent advances in ZnO nanostructured materials and their applications," *Nanotechnology*, vol. 30, no. 39, 2019.
[5] L. Vayssieres, "Growth of arrayed nanorods and nanowires of ZnO from aqueous solutions," *Advanced Materials*, vol. 15, no. 5, pp. 464–466, 2003.
[6] Z. L. Wang, "Zinc oxide nanostructures: Growth, properties and applications," *Journal of Physics: Condensed Matter*, vol. 16, pp. R829–R858, 2004.
[7] R. Wahab, S. G. Ansari, and Y. S. Kim, "Low temperature solution synthesis and characterization of ZnO nanoparticles," *Materials Research Bulletin*, vol. 42, pp. 1640–1648, 2007.
[8] Y. Wang, X. Jiang, and Y. Xia, "A solution-phase precursor route to SnO_2 nanowires," *Journal of the American Chemical Society*, vol. 125, no. 52, pp. 16176–16177, 2003.
[9] X. Chen and S. S. Mao, "Synthesis of SnO_2 nanomaterials for energy and environmental applications," *Chemical Reviews*, vol. 107, no. 7, pp. 2891–2959, 2007.
[10] A. Dieguez *et al.*, "The properties of tin oxide as a gas sensing material," *Sensors and Actuators B: Chemical*, vol. 109, pp. 1–7, 2005.
[11] B. D. Cullity and S. R. Stock, *Elements of X-Ray Diffraction*, 3rd ed. Upper Saddle River, NJ, USA: Prentice Hall, 2001.

[12] D. B. Williams and C. B. Carter, *Transmission Electron Microscopy: A Textbook for Materials Science*. New York, USA: Springer, 2009.
[13] J. I. Pankove, *Optical Processes in Semiconductors*. New York, USA: Dover, 1971.
[14] J. Xu *et al.*, "Enhanced photocatalytic activity of ZnO–SnO_2 heterojunction nanocomposites," *Applied Surface Science*, vol. 427, pp. 752–759, 2018.
[15] D. Zhang *et al.*, "Gas sensing properties of SnO_2/ZnO nanocomposites," *Sensors and Actuators B: Chemical*, vol. 190, pp. 371–377, 2014.
[16] K. M. Lwin *et al.*, "Synthesis and characterization of ZnO–SnO_2 nanocomposites," *Journal of Alloys and Compounds*, vol. 794, pp. 220–230, 2019.
[17] C. Wang *et al.*, "Metal oxide gas sensors: Sensitivity and influencing factors," *Sensors*, vol. 10, no. 3, pp. 2088–2106, 2010.
[18] P. Pascariu *et al.*, "ZnO-based nanomaterials for photocatalytic degradation," *Journal of Environmental Chemical Engineering*, vol. 4, no. 3, pp. 3215–3223, 2016.
[19] K. R. Raghupathi *et al.*, "Size-dependent antibacterial activity of ZnO nanoparticles," *Langmuir*, vol. 27, no. 7, pp. 4020–4028, 2011.